Ultrahigh near infrared photoresponsive organic field-effect transistors with lead

phthalocyanine/C$_{60}$ heterojunction on poly(vinyl alcohol) gate dielectric

Ultrahigh near infrared photoresponsive organic field-effect transistors with lead phthalocyanine/C$_{60}$ heterojunction on poly(vinyl alcohol) gate dielectric

Lei Sun[1], Jianping Zhang[1], Feiyu Zhao[1], Xiao Luo[1], Wenli Lv[1], Yao Ii[1], Qiang Ren[1], Zhanwei Wen[1], Yingquan Peng[1,2] and Xingyuan Liu[3]

[1] Institute of Microelectronics, School of Physical Science and Technology, Lanzhou University, South Tianshui Road 222#, Lanzhou 730000, People's Republic of China
[2] Key Laboratory for Magnetism and Magnetic Materials of the Ministry of Education, Lanzhou University, South Tianshui Road 222#, Lanzhou 730000, People's Republic of China
[3] State Key Laboratory of Luminescence and Applications, Changchun Institute of Optics, Fine Mechanics and Physics, Chinese Academy of Sciences, Changchun 130033, People's Republic of China

E-mail: yqpeng@lzu.edu.cn

CrossMark

Abstract

Performances of photoresponsive organic field-effect transistors (photOFETs) operating in the near infrared (NIR) region utilizing SiO$_2$ as the gate dielectric is generally low due to low carrier mobility of the channel. We report on NIR photOFETs based on lead phthalocyanine (PbPc)/C$_{60}$ heterojunction with ultrahigh photoresponsivity by utilizing poly(vinyl alcohol) (PVA) as the gate dielectric. For 808 nm NIR illumination of 1.69 mW cm^{-2}, an ultrahigh photoresponsivity of 21 A W^{-1}, and an external quantum efficiency of 3230% were obtained at a gate voltage of 30 V and a drain voltage of 80 V, which are 124 times and 126 times as large as the reference device with SiO$_2$ as the gate dielectric, respectively. The ultrahigh enhancement of photoresponsivity is resulted from the huge increase of electron mobility of C$_{60}$ film grown on PVA dielectric. AFM investigations revealed that the C$_{60}$ film grown on PVA is much smooth and uniform and the grain size is much larger than that grown on SiO$_2$ dielectric, which together results in four orders of magnitude increase of the field-effect electron mobility of C$_{60}$ film.

Keywords: PVA, gate dielectric, photoresponsivity, near infrared, photoresponsive organic field-effect transistors (photOFETs)

(Some figures may appear in colour only in the online journal)

1. Introduction

The past decades have witnessed tremendous progress of organic semiconductor devices. Organic semiconductors have many fundamental advantages compared with their inorganic counterparts such as lightweight, low-cost, large area flexible displays and etc [1–3]. Heterojunctions consisting of an electron-donating (donor) and an electron accepting (acceptor) materials have been widely used in the organic solar cells, photodiodes and ambipolar organic field effect transistors.

Excited states of organic molecules, or excitons, are characterized by large binding energies, typically on the order of 0.2–1.0 eV. The donor–acceptor interface has been proved to be essential for the efficient dissociation of photo generated excitons into free electrons and holes, which are then transported on the acceptor and donor molecules, respectively, producing the photocurrent [4].

Near infrared (NIR) photodetectors can be applied in many fields, like security, military and commercial applications [5, 6]. For light detection, organic photodiode (OPD)
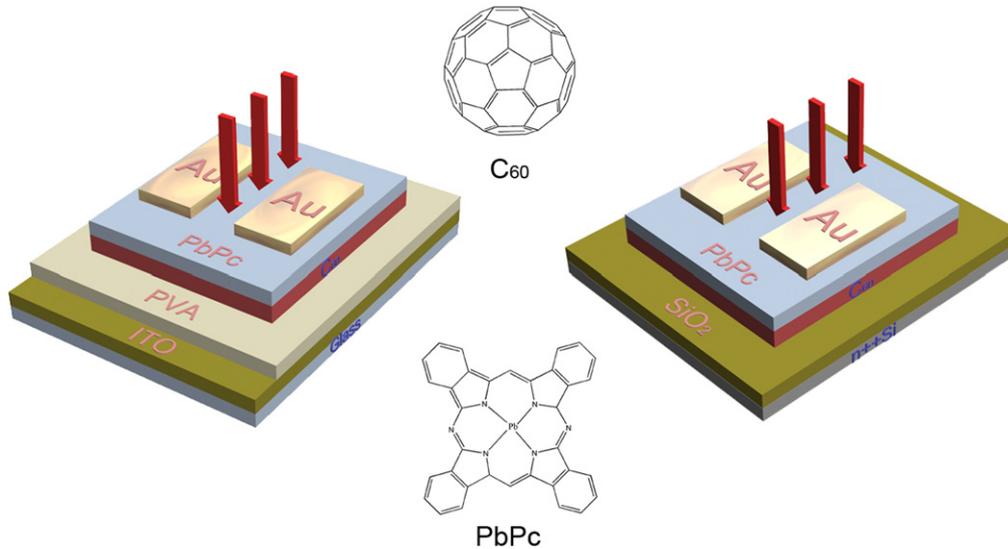
Figure 1. Schematic diagram of the device structure with PVA as gate dielectric (left) (device A) and SiO$_2$ as gate dielectric (right) (device B).
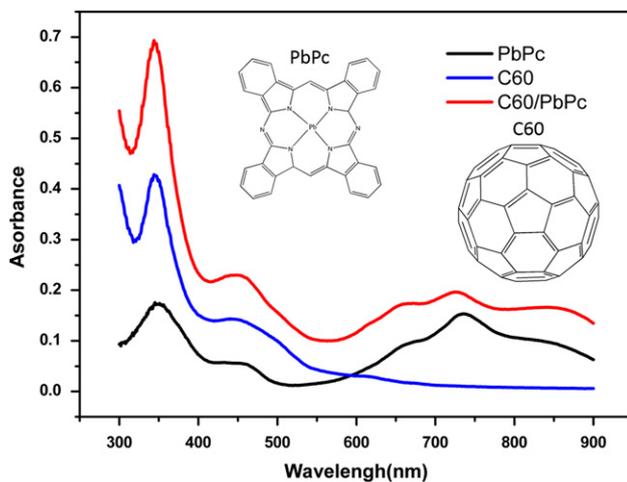
Figure 2. Absorption spectrum of PbPc (black line), C$_{60}$/PbPc heterojuction (red line) and C$_{60}$ thin film on quartz glass. The inset is molecular structure of C$_{60}$ and PbPc.

and photosensitive organic field-effect transistors have being intensively investigated. Traditionally, NIR OPDs were realized mainly by using NIR light sensitive narrow-energy-gap materials [7–10]. However for the active layer of high performance NIR OPDs, donor–acceptor planar- and bulk heterojunctions (BHJs) composed of a NIR sensitive p-type narrow-energy-gap molecule or polymer as the donor and a n-type molecule or polymer with low lying LUMO level as the acceptor were used [11–13]. Previous report by Wang *et al* on an OPD with CuPc:F16CuPc BHJ as the active layer showed a external quantum efficiency (EQE) of 9.22% for 808 nm NIR light, CuPc and F16CuPc denote copper phthalocyanine and copper hexadecafluorophthalocyanine, respectively [11]. X Gong group fabricated an OPD based on PCPDTBT:PCBM BHJ with an EQE of ~35% for 808 nm NIR light [13], PCPDTBT and PCBM denote poly[2, 6(4, 4-bis-(2-ethyl-hexyl)-4H-cyclopenta [2, 1-b:3, 4-b0]-dithiophene)- alt- 4,7-(2,

1, 3-benzothiadiazole)] and [6,6]-phenyl C61-butylyic acid methyl ester, respectively; by introducing PbS quantum dots into P3HT:PCBM BHJ, T Rauch *et al* obtained high photoresponsivity of 500 mA W^{-1} in the NIR region [14], P3HT denotes poly(3-hexylthiophene). In particular, F-C Chen group reported on an OPD by utilizing a three component BHJ as the active layer. Their OPD exhibited an EQE of ~500% and a photoresiponsivity of ~3000 mA W^{-1} in the NIR region [15].

Compared with OPDs, photOFETs have the advantage of higher photoresponsivity and lower noise. PhotOFETs operating in ultraviolet and visible light region has been reported much more than that in NIR region, which may be due to the low carrier mobilities of the NIR light sensitive organic materials [16]. Lead phthalocyanine (PbPc) is a p-type photosensitive molecule, and PbPc/C$_{60}$ heterojunction has been used in organic solar cells to extend the optical absorption into NIR region [17–19]. Recently, our group has reported on a photOFET based on a hybrid-planar BHJ containing PbPc, and a photoresponsivity as high as 322 mA W^{-1} was obtained for NIR light of 808 nm [16]. Except the photosensitive material, the performance of a photOFET intensively relies on the gate dielectric. Generally SiO$_2$ is used as the gate dielectric for their high quality and commercial availability [20, 21].

In this work, we report on an ultrahigh NIR sensitive photOFET based on PbPc/C$_{60}$ heterojunction utilizing poly (vinyl alcohol) (PVA) as the bottom gate dielectric. The device exhibited an ultrahigh photoresponsivity of ~21 A W^{-1} and EQE of ~3230% for NIR light of 808 nm at a gate voltage of 30 V and a drain voltage of 80 V. Physical origins of this ultrahigh photoresponsivity are investigated.

2. Experimental details

As shown in figure 1, bottom-gate top-contact geometry was used to fabricate the photOFETs, and two kinds of samples were fabricated in total. One is the high performance
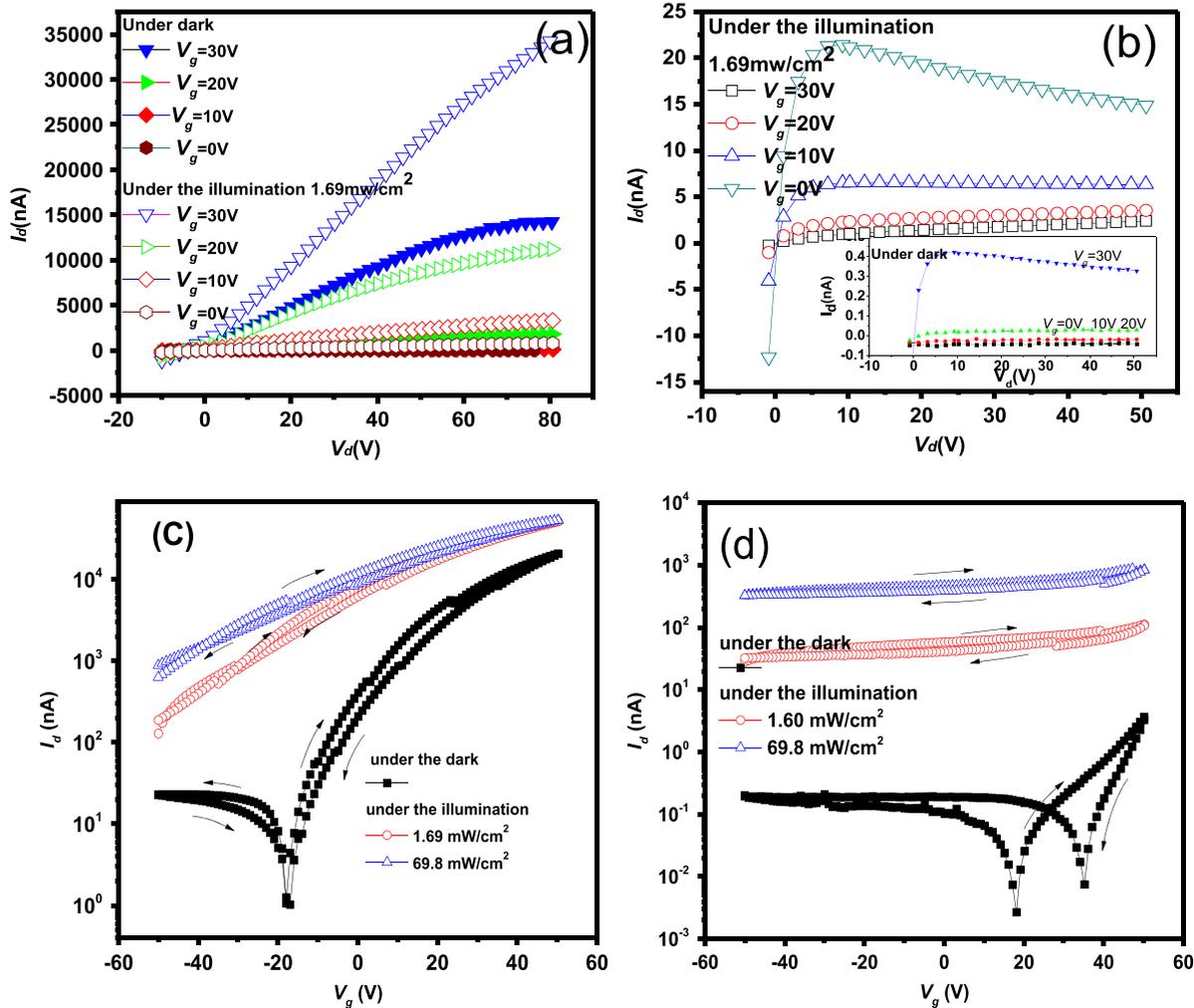
Figure 3. Output and transfer characteristics of device A(PVA as dielectric) (a), (c) and device B (SiO$_2$ as dielectric) (b), (d) under the illumination of 1.69 mW cm^{-2}. (In the figure 3(b) output charactaristics of device B under dark is inset).
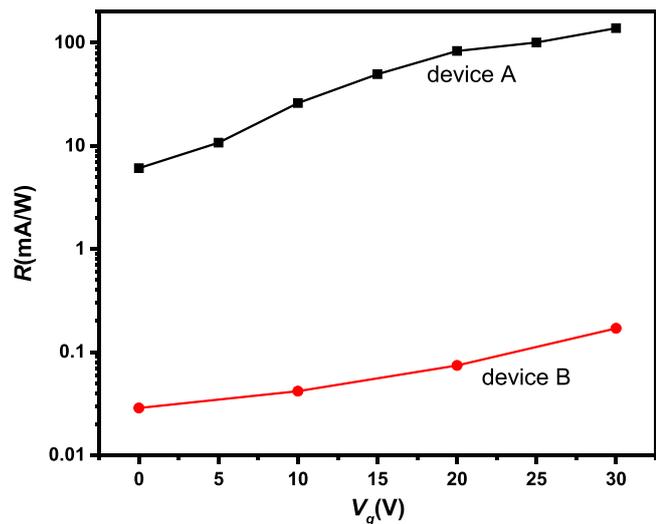
**Figure 4.** Plot of the photoresponsivity (*R*) versus gate voltage (*V$_g$*) for device A (PVA as dielectric) (filled squares) and device B (SiO$_2$ as dielectric) (filled circles) with $P_{opt} = 1.859 \times 10^{-3}$ mW and $V_d = 50$ V.

photOFET utilizing PVA as the dielectric (device A), while the other utilizing SiO$_2$ as the gate dielectric (device B) with the identical organic layer and top source and train contacts. device A and device B were fabricated on indium titanium oxide (ITO) coated glass and heavily n-type doped silicon with a thermally grown SiO$_2$ layer (capacitance per unit, $C_{ox} = 3.18$ nF cm^{-2}), respectively. ITO (in device A) and highly doped silicon (in device B) act as the gate electrodes, respectively. PVA was purchased from Alfa Aesar, C$_{60}$ from J & K Chemical Ltd, PbPc from Sigma-Aldrich, and were all used as received. ITO glass and Si substrates were cut into 15×15 mm in size and were cleaned with acetone ethanol and deionized water in an ultrasonic bath. After drying with N$_2$ gas blowing, ITO glasses and Si substrates were baked in an oven with a temperature 60 °C for 20 min. Then PVA solution (15% in water) was spun at 3000 rpm onto the top of ITO substrates forming thin film of 1100 nm with a capacitance per unit area of 4.24 nF cm^{-2}. And the films then were dried in vacuum atmosphere at 80 °C for 2 h. Si substrates were loaded into a vacuum oven with octadecyltrichlorosilane (OTS) atmosphere at the 120 °C temperature to allow a monolayer of OTS to self-assemble on the surface of SiO$_2$.
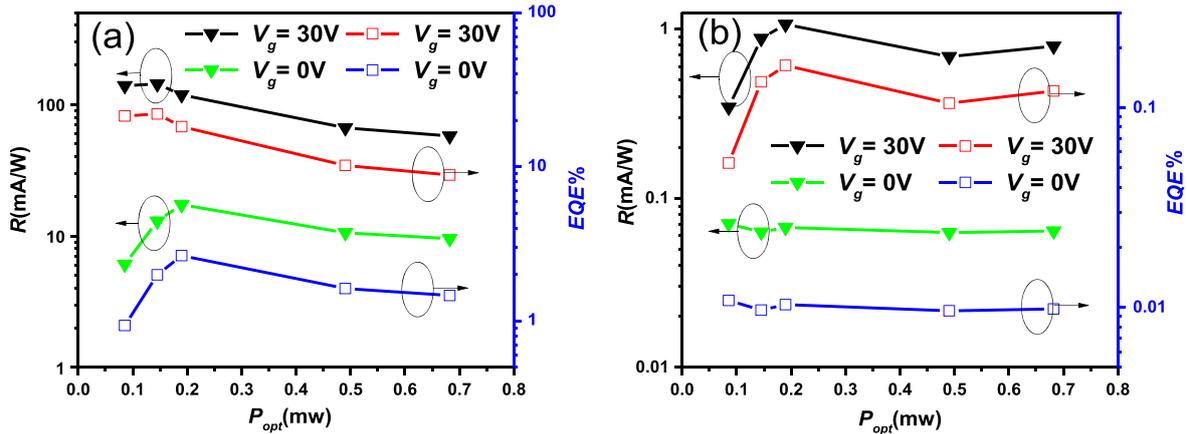
Figure 5. Plot of photoresponsivity (R) and external quantum efficiency (EQE) versus incident optical power (P_{opt}) for device A (a) and B (b) at $V_d = 50$ V, respectively, for gate voltage of 0 V and 30 V.
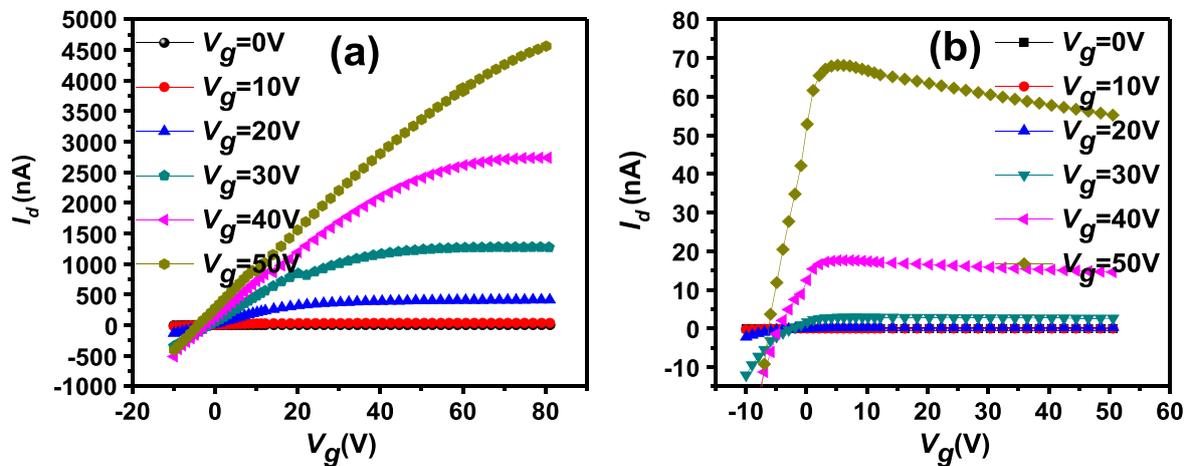
Figure 6. Output characteristics of single C_{60}-layer device with (a) PVA as the dielectric and (b) SiO_2 as the dielectric.

After a 50 nm thickness C_{60} film deposition on the top of PVA and SiO_2, another 20 nm thickness PbPc film was vacuum-deposited on the C_{60} layer in the vacuum of 3×10^{-3} Pa at a deposition rate of 0.02 nm s^{-1}, respectively. Au source/drain electrodes were thermally evaporated through a shadow mask which defined a channel length (L)/width (W) of 50 μm/3 mm. For the comparison of field-effect mobilities of C_{60} films grown on SiO_2 and PVA, single layer OFETs of the same C60 thickness with the structures of 'ITO/PVA/C_{60}/Au (S and D)' and 'n^+-Si/SiO_2/OTS/C_{60}/Au (S and D)' were simultaneously fabricated. S and D denotes source and drain electrodes. For convenience, they were denotes as PVA–C_{60}-OFET and SiO_2–C_{60}-OFET hereafter.

A laser diode of 808 nm wavelength was used for the photo effect measurements. The variation in light intensity was achieved using neutral density filters with various transmittances. All measurements were performed at room temperature.

3. Results and discussion

The absorptions of C_{60}, PbPc and double C_{60}/PbPc layers on quartz glass are depicted in figure 2. PbPc has an obvious absorption in the NIR and ultroviolet region and C_{60} has no absorption in the NIR but in the ultroviolet region. The absorption of double C_{60}/PbPc layer in the NIR originates mainly from PbPc.

Figure 3 shows the typical drain current–voltage characteristics and transfer characteristics of the photOFETs fabricated using PVA (device A) and SiO_2 (device B) as the dielectric layer both in the dark and under illumination, respectively. As seen in figures 3(a), (b), for both device A and reference device B, at a given drain voltage, the drain current increases with positive gate voltages, V_g, suggesting that both device A and device B are n-channel and operating in the accumulation mode. It is obvious that for a given drain voltage and gate voltage, the drain current either in the dark or under illumination of device A is much larger than that of device B. For example, at gate voltage, $V_g = 30$ V, drain voltage, $V_d = 50$ V, the drain current in the dark $I_{d,dark}$ of device B was only 0.327 nA, while that of device A was 10 400 nA, which is 3×10^4 times larger than that of device B. Under NIR light illumination with a roughly intensity of 1.69 mW cm^{-2} and at $V_g = 30$ V, $V_d = 50$ V, the drain current $I_{d,ill}$ of device B was only 14.9 nA, while that of device A was 22 300 nA, which is 1.5×10^3 times larger than that of device

Table 1. Device performance details. Values of saturation mobility and threshold voltage were extracted from the transfer curves by using equation (2) and experimental data.

Device	Structure	R (A W^{-1})	$\mu_{\text{dark,sat}}$ [a] (cm^2 V^{-1} s^{-1})	$\mu_{\text{ill,sat}}$ [b] (cm^2 V^{-1} s^{-1})	$V_{T,\text{dark,sat}}$ [c] (V)	$V_{T,\text{ill,sat}}$ [d] (V)
Device A	ITO/PVA/C$_{60}$/PbPc/Au (S and D)	21.0	2.77×10^{-1}	6.64×10^{-1}	6.80	6.77
Device B	n^+-Si /SiO$_2$/OTS/C$_{60}$/PbPc/Au (S and D)	0.166	2.41×10^{-5}	6.93×10^{-4}	28.7	14.3
PVA–C$_{60}$-OFET	ITO/PVA/C$_{60}$/Au (S and D)	—	2.48×10^{-2}	—	14.1	—
SiO$_2$–C$_{60}$-OFET	n^+-Si /SiO$_2$/OTS/C$_{60}$/Au (S and D)	—	1.79×10^{-3}	—	29.5	—

[a] $\mu_{\text{dark,sat}}$ denotes the saturation region mobility in the dark.
[b] $\mu_{\text{ill,sat}}$ denotes the saturation region mobility under the illumination of 1.69 mW cm^{-2}.
[c] $V_{T,\text{dark,sat}}$ denotes the saturation region threshold voltage in the dark.
[d] $V_{T,\text{ill,sat}}$ denotes the saturation region threshold voltage under the illumination of 1.69 mW cm^{-2}.
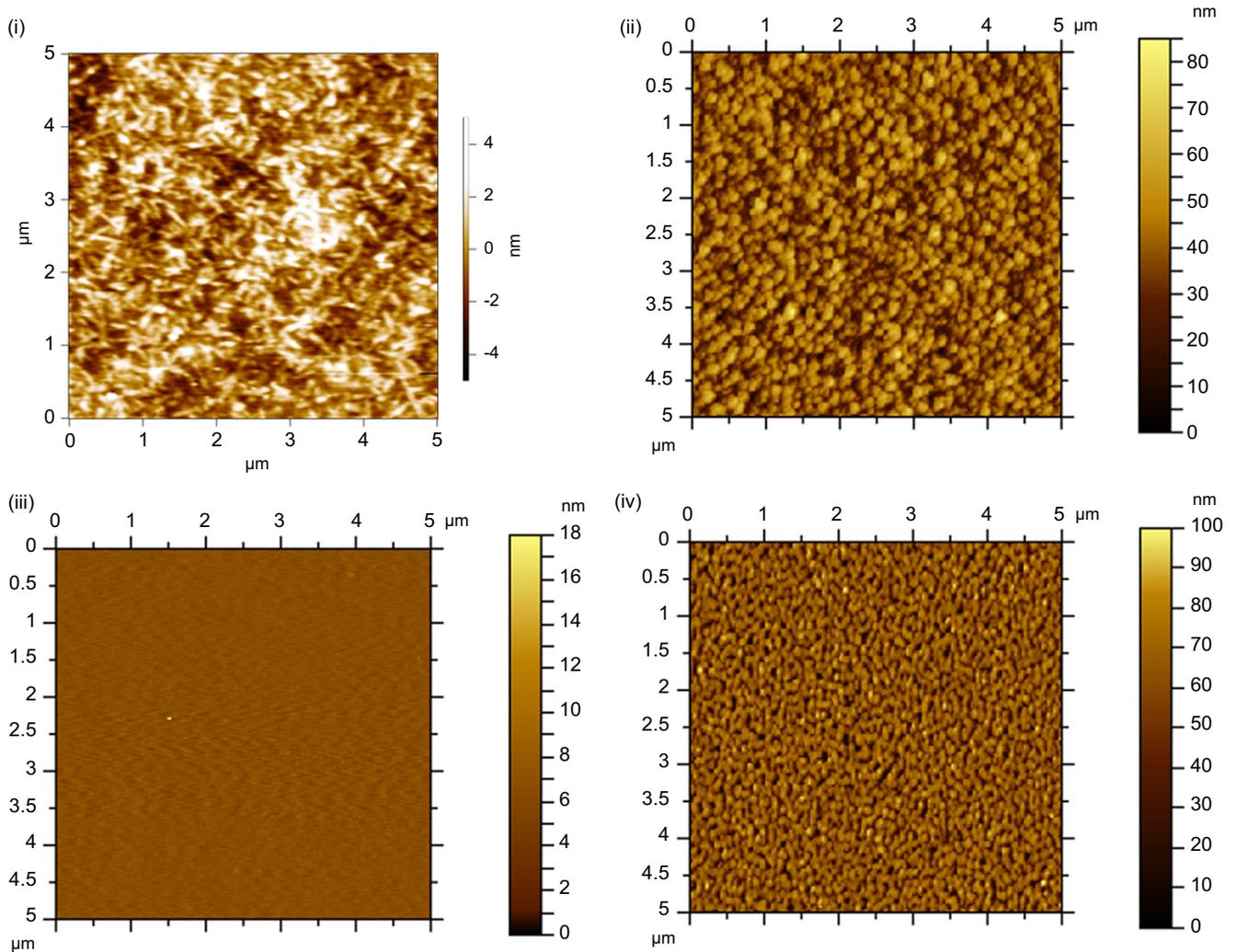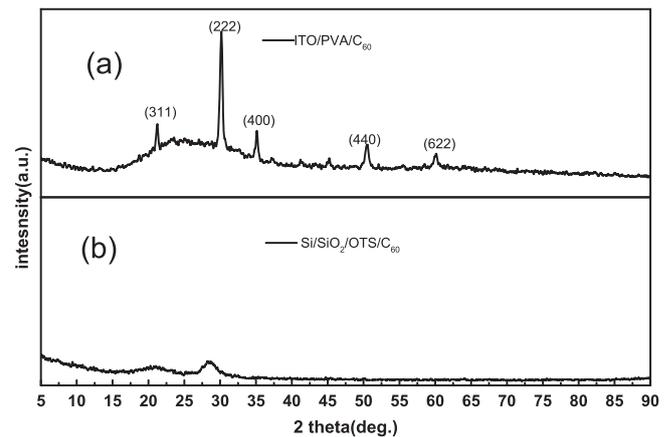
Figure 7. AFM 2D images of (i) 1.1 μm-PVA film on ITO coated glass, (ii) 50 nm-C_{60} film on last PVA–ITO coated glass, (iii) self-assembled OTS on SiO_2 substrate and (iv) 50 nm-C_{60} film on last OTS–SiO_2 substrate.

Table 2. AFM data obtained from surface analysis for PVA covered on ITO glass SiO_2 (OTS) on Si substrate C_{60} deposited on PVA C_{60} deposited on SiO_2 PbPc deposited on C_{60} and PbPc deposited on SiO_2.

Film	ITO/ PVA	ITO/ PVA	SiO_2/ OTS	SiO_2/ OTS/C_{60}
RMS[a](nm)	1.264	10.1	0.549	16.4

[a] RMS denotes root mean square height.

Figure 8. XRD patterns of the C60 films deposited on ITO/PVA(a) and Si/SiO2/OTS(b).

B. As seen in figures 3(c) and (d), the transfer characteristics was measured at $V_d = 80$ V for device A and $V_d = 50$ V for device B. The gate voltage V_g varied from −50 V to +50 V and then from +50 V to −50 V. For both device A and B, the drain current were enhanced with the increasing incident optical power. The hysteresis effects were observed in both device A and B. The difference of the threshold voltages in the two sweeping directions (forwards and backwards), i.e., $\Delta V_{th} = V_{th1} - V_{th2}$ was calculated. The ΔV_{th} of device A was smaller than that of device B (figures 3(c) and (d)). The hysteresis effects in the OFETs based on PVA are attributed

to the interface between PVA and organic semiconductor and/ or the high purity of PVA in other reports [22]. Different PVA purity level affects the hysteresis effects in the OFETs based on PVA. We supposed that the hysteresis effects in device A
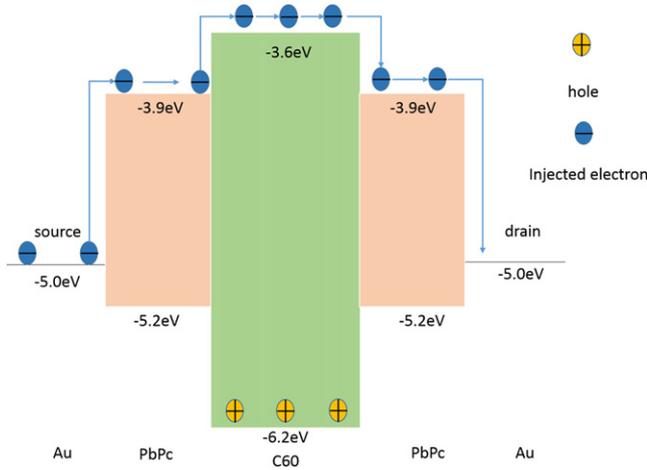
Figure 9. Energy diagram of the structure C_{60}/PbPc/Au.

was superior to that in device B due to the high purity of PVA (99%).

When illuminated, the PbPc layer, that is, photosensitive layer absorbs photons to generate excitions. Some of them diffused to a region with enough strong electric field will get dissociated and become free holes and electrons. C_{60} layer, that is, the carrier transport layer, transports the photogenerated free electrons to the electrode and PbPc layer, that is, the photosensitive layer, transports the photogenerated free holes to the other electrode under the influence of the electric field. An important parameter of a photOFET is the photoresponsivity, R, which is defined as the ratio of photocurrent I_{ph}, to the incident optical power P_{opt}, that is $R = I_{ph}/P_{opt}$. From the photoresponsivity, R, the external quantum efficiency, EQE, can be determined via the expression

$$EQE = \frac{hc}{q\lambda} R. \tag{1}$$

Here h, c and q are the Planck constant, the velocity of light in vacuum and the elementary electric charge, respectively; λ is the wavelength of incident light.

Figure 4 shows the gate voltage depended photoresponsivity for both device A and device B at $V_d = 50$ V. The photoresponsivities and EQE increase with the gate voltage. At zero gate voltage, the responsivity of device B was 0.0287 mA W^{-1}, while that of device A was 6.096 mA W^{-1}, which is 212 times larger than that of device B. At $V_g = 30$ V, the responsivity of device A reaches 139 mA W^{-1}, which is 817 times larger than that at device B (0.170 mA W^{-1}). At further higher operation voltages of $V_g = 30$ V and $V_d = 80$ V, device A reached a ultrahigh responsivity of 2100 mA W^{-1} and an EQE of 3230%. These values are much larger than that reported in literatures, and in particular, they are several times larger than the record values reported in [15].

Figure 5 shows the dependence of photoresponsivity on the incident optical power and EQE of device A and device B at $V_d = 50$ V. For both devices, as P_{opt} increasing, R and EQE first increase and reach a maximum, R_{max} at a certain $P_{opt,max}$, and then decrease. It is to note that both R_{max} and $P_{opt,max}$ are

gate and drain voltage dependent. The R and EQE of device A are about 2 orders of magnitude larger than that of device B.

The charge transport ability of an OFET is characterized by the saturation region mobility (μ_{sat}), which are generally extracted by equation (2):

$$I_d = \frac{1}{2} \mu_{sat} C_i \frac{W}{L} \left(V_g - V_{th} \right)^2 \quad V_d > \left(V_g - V_{th} \right), \tag{2}$$

Here μ_{sat} is the saturation region mobility, V_{th} is the threshold voltage, W and L are the channel width and length respectively. C_i is the capacitance per unit area of the gate dielectric layer.

The ultrahigh photoresponsivity of device A originates from high electron field-effect mobility of C_{60}-OFET grown on PVA dielectric. As shown in figure 6, the drain current I_d of C_{60} OFET grown on PVA dielectric is several ten times larger than that of grown on SiO$_2$ dielectric. At $V_g = V_d = 50$ V, the drain current I_d of PVA–C_{60}-OFET is approximately 60 times larger than that of SiO$_2$–C_{60}-OFET. The μ_{sat} of SiO$_2$–C_{60}-OFET was 1.87×10^{-3} cm^2 V^{-1} s^{-1}, while that of PVA–C_{60}-OFET was 2.48×10^{-2} cm^2 V^{-1} s^{-1}, which is 13 times larger than that of the SiO$_2$–C_{60}-OFET. The performance details of the devices displays in table 1.

Charge carrier mobility of a thin film is strongly dependent on its surface morphology and crystal structure. It is established that for thin films of poly crystal structure, the carrier mobility increases with the grain size. To elucidate the cause of the increase of electron field-effect mobility in PVA–C_{60}-OFET, the morphology of the surfaces of PVA films grown on ITO glass, PVA film grown on SiO$_2$, C_{60} film on PVA, C_{60} film on SiO$_2$, PbPc film on PVA/C_{60}, and PbPc film on SiO$_2$/C_{60} are characterized by means of atoms force microscopy (AFM, Angilent 5500) operating in tapping mode. As shown in figure 7, although the surface roughness of ITO/PVA is 1.264 nm, which is larger than that of SiO$_2$/OTS (0.549 nm), the surface roughness of ITO/PVA/C_{60} of 10.1 nm is much smaller than that of SiO$_2$/OTS/C_{60} (16.4 nm). In addition, the grain size C_{60} film on ITO/PVA is much larger than that SiO$_2$/OTS/C_{60}, which is solid evidence of higher mobility of C_{60} film grown on ITO/PVA film than that on SiO$_2$/OTS. The AFM detail information of the films in the devices is in table 2.

Figure 8 shows the x-ray diffraction (XRD, Rigaku D/max-2400) patterns of C_{60} films deposited on PVA and SiO$_2$, respectively. According to phase analysis of C_{60} films, the diffraction peaks at 21.2°, 30.17°, 35.1°, 50.52° and 60.05° were assigned to (311), (222), (400), (440) and (622) lines respectively in figure 8(a) while almost no diffraction peak was observed in figure 8(b). The observed characteristic peak of C_{60} film on PVA at 21.2° in figure 8(a) (no diffraction peak was observed at 21.2° in figure 8(b)) indicated that the C_{60} film grown on PVA has higher crystallinity than that on SiO$_2$/OTS/C_{60}.

The effect of PbPc layer on device mobility can be understood with the help of theory of conduction in organic device [23]. PbPc layer has two effects on the electron transport in the device: (1) as shown in figure 9, the LUMO of PbPc lies between that of C_{60} and Fermi level of source electrode, PbPc function as source/drain electrode buffer layer
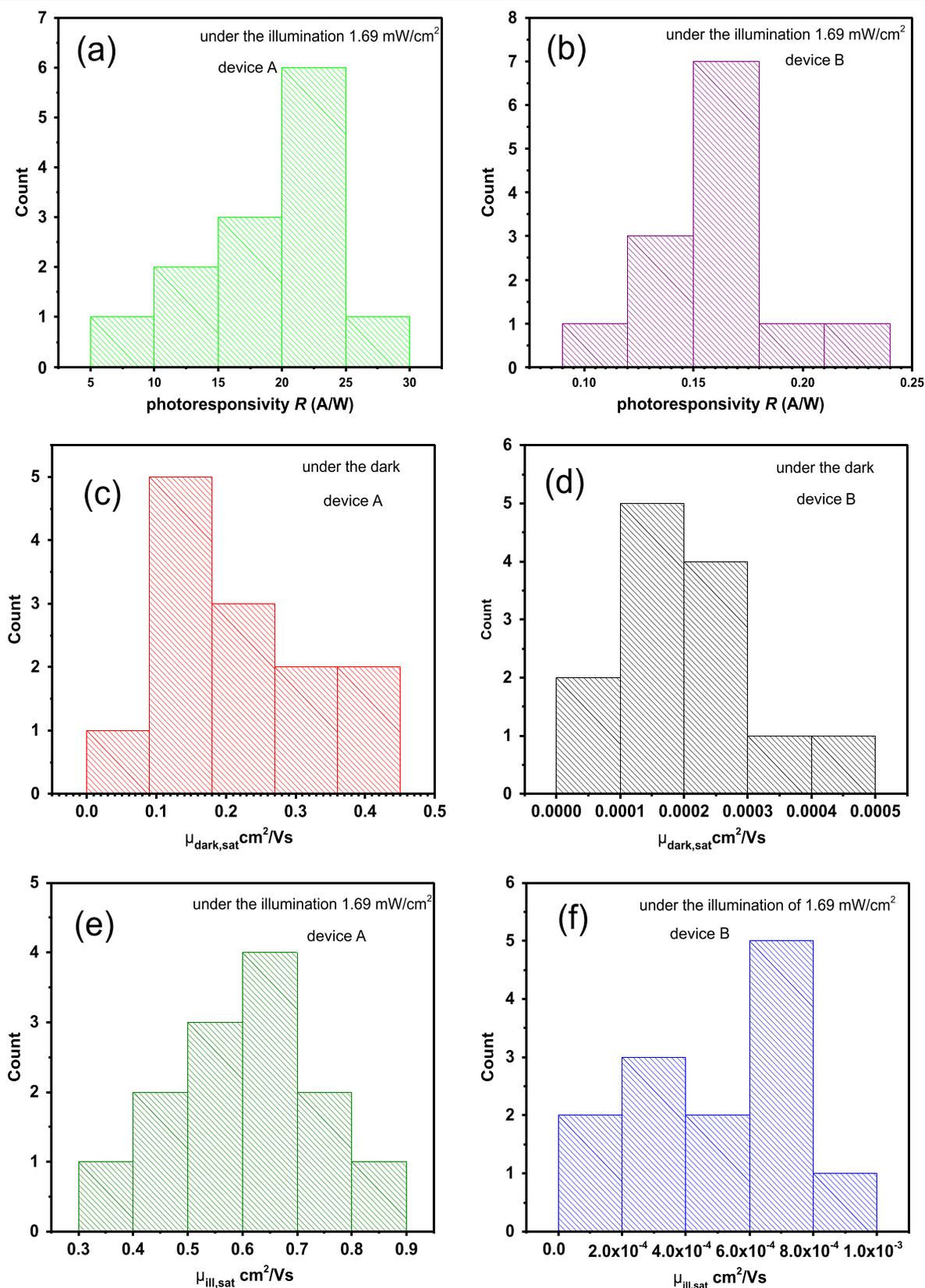
Figure 10. Statistical analysis of electrical characteristics: photoresponsivity *R* of device A(a) and device B(b), mobility of device A under the dark(c) and device B under the dark (d), mobility of device A under the illumination of 1.69 mW cm^{-2} (e) and device B under the illumination of 1.69 mW cm^{-2} (f) respectively.

Table 3. Statistical analysis of device A and B electrical characteristics details.

Device	R_{max}[a] (A W^{-1})	R_{min}[a] (A W^{-1})	R_{mean}[a] (A W^{-1})	R_{SD}[a] (A W^{-1})
Device A	25.7	7.58	16	2.85
Device B	0.255	0.110	0.173	0.093

Device	$\mu_{dark,\,sat,\,max}$[b] (cm^2 V^{-1} s^{-1})	$\mu_{dark,\,sat,\,min}$[b] (cm^2 V^{-1} s^{-1})	$\mu_{dark,\,sat,\,mean}$[b] (cm^2 V^{-1} s^{-1})	$\mu_{dark,\,sat,\,SD}$[b] (cm^2 V^{-1} s^{-1})	$\mu_{ill,\,sat,\,max}$[c] (cm^2 V^{-1} s^{-1})	$\mu_{ill,\,sat,\,min}$[c] (cm^2 V^{-1} s^{-1})	$\mu_{ill,\,sat,\,mean}$[c] (cm^2 V^{-1} s^{-1})	$\mu_{ill,\,sat,\,SD}$[c] (cm^2 V^{-1} s^{-1})
Device A	3.9×10^{-1}	7.05×10^{-2}	2.10×10^{-1}	1.24×10^{-1}	8.10×10^{-1}	9.75×10^{-2}	4.65×10^{-1}	2.73×10^{-1}
Device B	5.79×10^{-4}	1.91×10^{-5}	2.57×10^{-4}	1.12×10^{-4}	8.82×10^{-4}	1.63×10^{-4}	4.01×10^{-4}	6.98×10^{-5}

[a] R_{max}, R_{min}, R_{mean}, R_{SD} denote the maximum photoresponsivity, minimum photoresponsivity, mean photoresponsivity and SD of photoresponsivity respectively.

[b] $\mu_{dark,sat,max}$, $\mu_{dark,sat,min}$, $\mu_{dark,sat,mean}$, $\mu_{dark,sat,SD}$ denote the maximum saturation mobility, minimum saturation mobility, mean saturation mobility and SD of saturation mobility under the dark respectively.

[c] $\mu_{ill,sat,max}$, $\mu_{ill,,sat,min}$, $\mu_{ill,,sat,mean}$, $\mu_{ill,sat,SD}$ denote the maximum saturation mobility, minimum saturation mobility, mean saturation mobility and SD of saturation mobility under the illumination of 1.69 mW cm^{-2} respectively.

which facilitates electron injection from source electrode into C_{60} channel layer. That is buffer layer effect increases the channel current and thus the carrier mobility of the device; (2) as PbPc is a p-type organic semiconductor, its electron mobility is very low, so it function as a large resistance for electron conduction, that is, PbPc layer reduces the mobility of device. For device A, with PVA as gate dielectric the conductivity of C_{60} channel is high, so the current conduction from the source the source to the drain electrode is limited by electron injection at the source. We suggest, the positive contribution of PbPc as buffer layer is larger than the negative contribution as resistance, which results in the increase of device mobility. For device B, with SiO_2 as the dielectric the conductivity of C_{60} channel is low, so the current conduction from the source to the drain electrode is limited by the bulk resistance of the channel. The negative contribution of PbPc as resistance is larger than the positive contribution as buffer layer, which results in the decrease of device mobility.

We repeated the same series of experiments more than three times. In these experiments, the trend was invariant, although absolute values of device parameters varied slightly in each series. The distribution and uniformity of device parameters photoresponsivity R, saturation mobility under dark $\mu_{sat,dark}$ and saturation mobility $\mu_{sat,ill}$ under illumination of $1.69 \, mW \, cm^{-2}$ are shown in figure 10. Statistical analysis of device A and B electrical characteristics details are presented in table 3. The standard deviation(SD) of device A is larger that of device B for every device parameter. Although the distribution and uniformity of device parameters for device A is inferior to that for device A, the detail property of device A is superior to that of device B as mentioned-above.

In addition, photOFETs based on polyvinyl pyrrolidone (PVP) as dielectric was also fabricated. The overall performance of photOFETs based on PVP was inferior to that of device A but superior to that of device B. For example, the photo-responsivity R is $0.3 \, A \, W^{-1}$ which is between those of device A and B. These results reveals that organic polymer dielectric has much better properties than inorganic dielectric which needs more specific research. In the next work, we will concentrate much more on organic polymer dielectric in photOFETs.

4. Conclusions

In conclusion, ultrahigh NIR responsive photOFETs based on PbPc/C_{60} heterojunction utilizing PVA as the dielectric (device A) were fabricated and characterized. For 808 nm NIR illumination of $1.69 \, mW \, cm^{-2}$, ultrahigh photo-responsivity of $21 \, A \, W^{-1}$, and EQE of 3230% were obtained at $V_g = 30 \, V$ and $V_d = 80 \, V$, which are 124 times and126 times as large as the reference device with SiO_2 as the gate dielectric, respectively. The achieved ultrahigh responsivity and EQE are several times larger than the record values reported in literature. The ultrahigh enhancement of photo-responsivity is resulted from the huge increase of electron mobility of C_{60} film grown on PVA dielectric. AFM investigations revealed that the C_{60} film grown on PVA is much

smooth and uniform and the grain size is much larger than that grown on SiO_2 dielectric and XRD investigations demonstrated that C60 film grown on ITO/PVA has higher crystallinity than that grown on SiO_2/OTS/C_{60}, which together resulted an 11493 times increase of field-effect electron mobility of C_{60} film.

References

[1] Park Y, Han K S, Lee B H, Cho S, Lee K H, Im S and Sung M M 2011 *Org. Electron.* **2** 348–52
[2] Park Y W 2010 *Chem. Soc. Rev.* **7** 2352–3
[3] Lee S, Yeo J S, Ji Y, Cho C, Kim D Y, Na S I, Lee B H and Lee T 2012 *Nanotechnology* **34** 344013
[4] Heremans P, Cheyns D and Rand B P 2009 *Acc. Chem. Res.* **11** 1740–7
[5] Levine B F 1993 *J. Appl. Phys.* **8** R1
[6] Chen C J, Choi K K, Chang W H and Tsui D C 1998 *Appl. Phys. Lett.* **1** 7
[7] Pandey R, Kerner R A, Menke S M, Holst J, Josyula K V B and Holmes R J 2013 *Org. Electron.* **3** 804–8
[8] Zimmerman J D, Yu E K, Diev V V, Hanson K, Thompson M E and Forrest S R 2011 *Org. Electron.* **5** 869–73
[9] Wei Y, Ma W, Huang J, Zhang Y, Huo Y, Cui K, Chen L and Shi Y 2011 *Appl. Phys. Lett.* **10** 103507
[10] Diev V V, Hanson K, Zimmerman J D, Forrest S R and Thompson M E 2010 *Angew. Chem., Int. Ed. Engl.* **32** 5523–6
[11] Wang J B, Li W L, Chu B, Lee C S, Su Z S, Zhang G, Wu S H and Yan F 2011 *Org. Electron.* **1** 34–8
[12] Binda M, Iacchetti A, Natali D, Beverina L, Sassi M and Sampietro M 2011 *Appl. Phys. Lett.* **7** 73303
[13] Liu X, Wang H, Yang T, Zhang W, Hsieh I and Cheng S Z D 2012 *Org. Electron.* **12** 2929–34
[14] Rauch T, Böberl M, Tedde S, Fürst J, Kovalenko M, Hesser G, Lemmer U, Heiss W and Hayden O 2009 *Nat. Photonics* **3** 332–6
[15] Chuang S, Chien S and Chen F 2012 *Appl. Phys. Lett.* **1** 13309
[16] Peng Y, Lv W, Yao B, Fan G, Chen D, Gao P, Zhou M and Wang Y 2013 *Org. Electron.* **4** 1045–51
[17] Tiwari S P, Potscavage W J, Sajoto T, Barlow S, Marder S R and Kippelen B 2010 *Org. Electron.* **5** 860–3
[18] Hiramoto M, Kitada K, Iketaki K and Kaji T 2011 *Appl. Phys. Lett.* **2** 23302
[19] Jung Kim H, Shim H, Whan Kim J, Hwi Lee H and Kim J 2012 *Appl. Phys. Lett.* **26** 263303
[20] Yadav S and Ghosh S 2014 *Phys. Semicond. Devices* **33** 905–6
[21] Liu Z, Zhao J, Xu W, Qian L, Nie S and Cui Z 2014 *ACS Appl. Mater. Interfaces* **13** 9997–10004
[22] Egginger M, Irimia-Vladu M, Schwödiauer R, Tanda A, Bauer2 S and Sariciftci S 2008 *Mater. Res. Soc. Symp. Proc.* **1091** AA11–46
[23] Peng Y and Yang J 2005 *Appl. Phys. A* **80** 1511–6